MATEC Web of Conferences **33**, 01001 (2015)
DOI: 10.1051/matecconf/20153301001

Atom probe tomography reveals options for microstructural design of steels and titanium alloys by segregation engineering

D. Raabe[a], M. Herbig, M. Kuzmina, S. Sandlöbes, Z. Tarzimoghadam, D. Ponge

Max-Planck-Institut für Eisenforschung GmbH, Max-Planck-Str. 1, 40237 Düsseldorf, Germany

Abstract. Here we discuss approaches for designing microstructures in steels and titanium alloys by manipulating the segregation content and the structural state of lattice defects. Different mechanisms can be utilized in that context, such as for instance site specific segregation as described by the Gibbs isotherm and the generalized defectant concept, confined phase transformation phenomena and the formation of complexions, i.e. confined chemical and structural states at lattice defects.

1 Segregation engineering and complexions

Lattice defects in metallic alloys are amenable to chemical and structural manipulation, not only in the form of kinetic transients but also due to equilibrium effects. Several mechanisms have been discussed in that context. Gibb's classical isotherm, like the re-formulations by McLean and Langmuir, describe the reduction in energy of solid solutions when segregation to lattice defects (originally described for surfaces and internal interfaces) leads to a reduction of their self-energy (e.g. grain boundary energy) [1-3]. Kirchheim's defectant concept generalizes this principle by stating that all types of lattice defects are in principle amenable to equilibrium segregation in solid solutions when the energy of the defect affected is reduced [4]. The complexion concept carries this idea further: It describes confined chemical and structural states at planar defects which are distinctly different from those of the abutting bulk volume [5-11]. Like in the Gibbs concept the driving force for this kind of confined state at an interface, referred to as complexion, is due to the fact that it reduces its self-energy. Thus, the complexion concept extends the Gibbs isotherm also to non-isostructural defect states. This means that both, the classical isotherm or, more generally, defectant states and complexions can only exist at lattice defects.

Besides these confined types of chemical and structural changes of lattice defects also conventional phase transformation and phase growth can occur at segregation decorated internal defects when the system is (in some cases locally) rendered into the two-phase regime. Here, we provide some examples how these different types of segregation phenomena and confined structural states at lattice defects can be used to design complex microstructures in metallic alloys by using simple heat treatments [12-14]. We give examples of corresponding segregation effects, complexions and phase transformation phenomena in Fe-Mn steels taken from earlier work [12-19]. Also, we present some related phenomena in the system Ti-Mo.

The main idea behind the concept of segregation engineering is to use the mechanisms described above for manipulating microstructures in a beneficial way rather than accepting solid decoration of lattice defects as an undesired side effect of conventional heat treatments.

[a] Corresponding author: d.raabe@mpie.de

2 Segregation to dislocations and low-angle grain boundaries in Fe-Mn steels

As an example of segregation engineering to linear defects we studied decoration of Mn to dislocations in martensitic Fe-Mn steels, Figure 1 [19]. The Fe-9wt% Mn solid solution was melted in a vacuum induction furnace from high purity ingredients. A slab was cast as a 4 kg rectangular billet. The slab edges were trimmed.

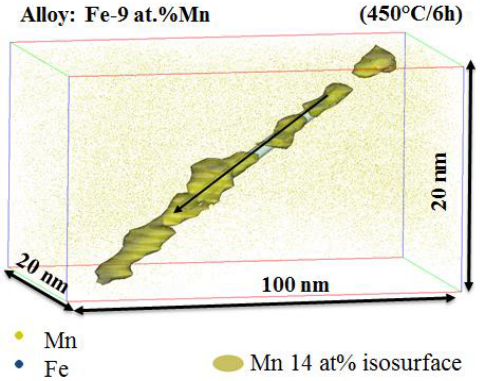

Figure 1. Different defects and associated segregation and complexion states were observed in Fe-9wt.% Mn. Here, a Mn decorated dislocation is shown. The sample was homogenized, 50% cold-rolled and heat treated at 450°C for 6h [19].

Homogenization annealing was conducted at 1100 °C followed by water quenching. The alloy was then cold-rolled to a thickness reduction of 50% using multiple passes for increasing the dislocation density. Samples were reheated to different temperatures between 400°C and 540°C for 6, 18 and 336 hours (2 weeks), respectively. After these heat treatments both, strong segregation of more than 25 at.% Mn at 450°C and confined structural face centered cubic states with substantial long term stability were observed at single dislocations [19].

Correlated structural and chemical characterization was conducted by using Atom Probe Tomography (APT) and Transmission Electron Microscopy (TEM) both, individually, as well as on the same sample, Figure 2. The APT samples were prepared using a FEI Helios NanoLab600i dual-beam Focused Ion Beam / Scanning Electron Microscopy instrument. APT was performed on a LEAP 3000X HR device by Imago Scientific Instruments at a set-point temperature of 50 K in laser mode with 532 nm wavelength, ~10 ps pulse width, 250 kHz pulse frequency and 0.4 nJ pulse energy. Details of the synthesis and analysis procedures are given elsewhere [19].

Figure 1 shows an example of a Mn-decorated dislocation which in part reaches Mn concentrations that match the equilibrium concentration in austenite at the applied heat treatment temperatures (400°C– 500°C). This observation indicates that local segregation might trigger the formation of locally confined chemical and structural austenitic states inside a surrounding martensitic matrix. Some of these local fcc states observed at the dislocation cores remained stable during heat treatments of up to 2 weeks at 450°C.

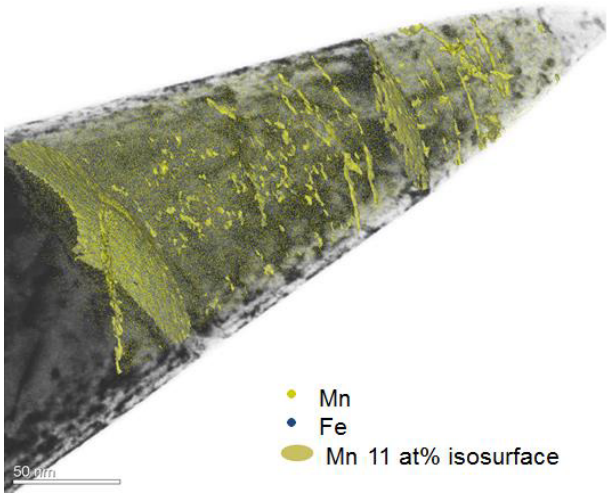

Figure 2. Correlated structural and chemical characterization was conducted by using Atom Probe Tomography (APT) and Transmission Electron Microscopy (TEM) in Fe-9wt.% Mn. The image reveals Mn decorated dislocations and low angle grain boundaries. The sample was homogenized, 50% cold-rolled and heat treated at 450°C for 6h [19].

Very similar effects were observed for Mn-decorated low angle grain boundaries such as shown in Figure 2. Correlated microscopy in this case revealed that particularly the edge dislocation components were heavily decorated by up to 25at.% Mn while the screw dislocation components revealed no segregation content. Similar as observed for isolated dislocations also some of the low angle grain boundaries revealed such confined chemical and structural states at the dislocation cores. In some cases these states remained stable in size and composition through an annealing time of 18 h (Figure 3) and even over two weeks at 450°C. This did not apply to all grain boundaries studied though.

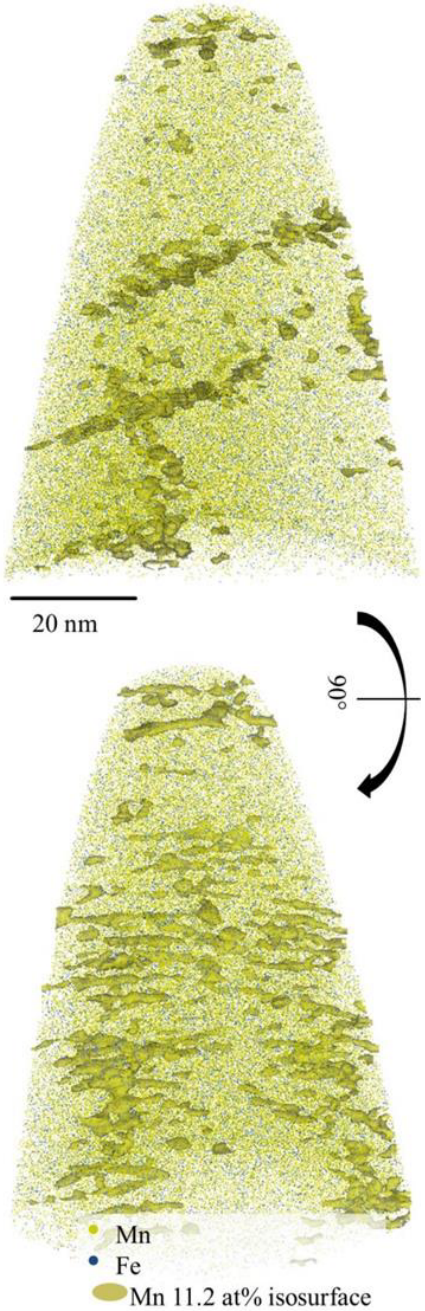

Figure 3. Atom probe tomography (APT) analysis of decorated dislocations in a Fe-9wt.% Mn alloy, viewed from two different sides. The sample was homogenized, 50% cold-rolled and heat treated at 450°C for 18h. In some cases the confined chemical and structural states observed at the dislocations and low angle grain boundaries did not grow further during this extended heat treatment.

The associated mechanical properties of the heat treated martensitic alloys are still under investigation and will be discussed in more detail in a subsequent publication. It is observed, however, that the segregation effects and the confined chemical and structural states observed at many of the isolated dislocations and also at many of the low angle grain boundaries become also apparent in the form of serrated plastic flow phenomena and distinct mechanical yield strength peaks at the beginning of deformation in corresponding ambient temperature tensile tests.

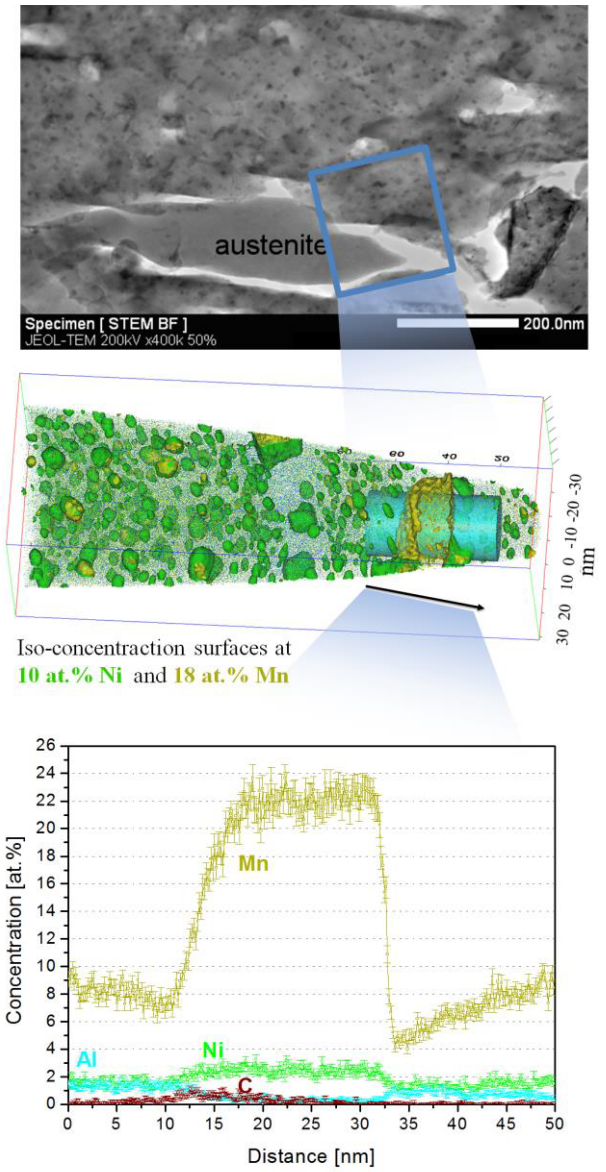

Figure 4. Joint TEM and atom probe tomography analysis of a decorated and phase transformed region in a Fe-12wt.% Mn based maraging steel, containing also nano-sized intermetallic precipitates inside the cubic martensite phase. The sample was homogenized and heat treated at 450°C for 48h. The data were taken from a preceding paper [12,13,16]. In this case no complexion was formed but instead regular confined phase transformation (reversion) from the martensite into the austenite. Unlike some of the complexion states mentioned above these regions could grow further upon prolonged heat treatment.

Figure 4 shows an example where local segregation in a Fe–Mn maraging steel did not lead to permanently confined chemical and structural states such as reported above but rather to conventional phase transformation from the cubic martensite into the austenite at the Mn-decorated grain boundary. The martensitic phase is visualized through the presence of multiple nano-sized intermetallic precipitates which formed upon heat treatment at 450°C for 48h. The results are taken from earlier publications [12,13,16]. The design of such martensitic maraging steels, containing also regions where martensite to austenite reversion occurred after preceding massive Mn segregation, was the basis for the development of the so-called maraging TRIP steels. This means that the transformed regions can be subject to transformation induced plasticity phenomena.

These examples of segregation engineering show that the different phenomena observed must be carefully differentiated. In some cases ordinary segregation in the Gibbs isotherm sense and also equilibrium phase transformation phenomena were observed. In other cases confined segregation entailed changes in the structural state of the lattice defect, however, without rendering the surrounding matrix also into the same state. This means that we observed in some cases confined chemical and structural states after segregation which did neither resemble conventional segregation phenomena (where no structure change occurs) nor conventional phase transformation (where the phase would grow upon further heat treatment). These different mechanisms are currently still under investigation [19].

3 Segregation and confined phase states in Ti-Mo alloys

Solid solution alloys based on Ti and minor additions of Mo, Nb, Fe or V reveal some similarities to steels: they show pronounced segregation effects and a variety of diffusional and athermal phase transformation phenomena between the hexagonal and the body centered cubic phases [20]. More specific, we present some recent results obtained on a plain binary Ti-4Mo (wt.-%) model alloy where we found different types of diffusion driven allotropic phase transformations and shear and / or diffusion dominated modes of martensitic transformations, enabling to realize a wide variety of efficient ways to design microstructures. The data presented here are taken from a recent publication [20].

Figure 5 shows an example where in a homogenized, water quenched and subsequently 950°C-550°C heat treated Ti-4Mo (wt.-%) solid solution model alloy pronounced elemental partitioning between a zone of hexagonal matrix α and an abutting zone of body centered cubic β is observed. The TEM analysis reveals very thin (10-25 nm thickness) bcc regions which are embedded between the hexagonal acicular matrix crystals. The water quench creates shear-dominated martensite and the subsequent tempering leads to the decomposition and Mo partitioning according to $\alpha' \rightarrow \alpha + \beta$. These thin ß-layers at the interfaces increase the toughness of the material [20].

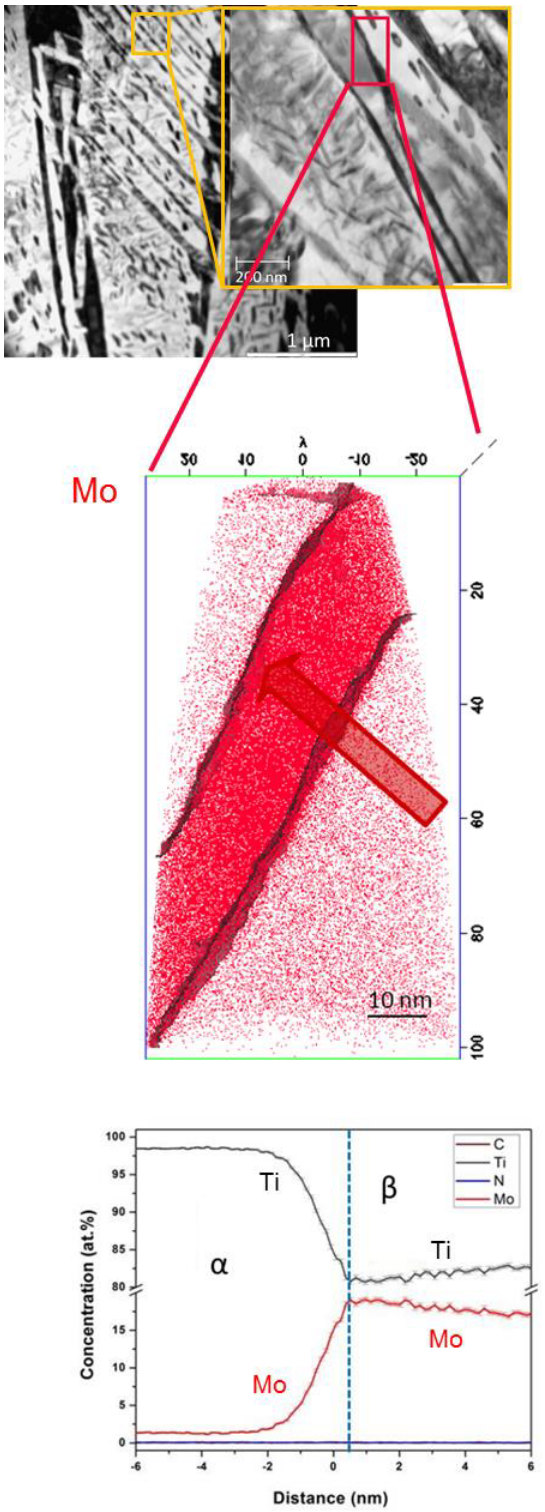

Figure 5. Segregation effect driven by Mo partitioning in a Ti-4wt.% Mo solid solution model alloy. Bright-field TEM imaging revealing a region containing a zone of hexagonal matrix α and an abutting zone of body centered cubic β. The latter phase is rich in Mo. The microstructure was designed by imposing a solution heat treatment at 950°C in the β regime, followed by water quenching and a subsequent annealing treatment at 550°C. The APT elemental map and the corresponding 1-D concentration profile (bin width 0.5 nm) across the Mo enriched layer reveal the spatial distribution of the Mo atoms [20].

References

1. J.W. Gibbs, The Collected Works of J. Willard Gibbs Vol. 1, Yale University Press, New Haven, CT (1948)
2. I. J. Langmuir, Am Chem Soc **40**, 1361 (1918)
3. D. McLean, Grain Boundaries in Metals. Oxford: Oxford University Press (1957)
4. R. Kirchheim, Acta Mater **55**, 5129 (2007)
5. M. Tang, W. C. Carter, R. M. Cannon, Phys. Rev. Lett. **97**, 075502 (2006)
6. M. Tang, W. C. Carter, R. M. Cannon Phys Rev B **73**, 024102 (2006)
7. S. J. Dillon, M. Harmer, Acta Mater **55**, 5247 (2007).
8. S. J. Dillon, M. Tang, W. C. Carter, M. P. Harmer, Acta Mater. **55**, 6208 (2007)
9. M. P. Harmer, Science **332**, 182 (2011)
10. M. Baram, D. Chatain, W. D. Kaplan, Science **332**, 206 (2011)
11. W. Kaplan, D. Chatain, P. Wynblatt, W. C. Carter, J Mater Sci **48**, 5681 (2013)
12. D. Raabe, S. Sandlöbes, J. Millán, D. Ponge, H. Assadi, M. Herbig, P.-P. Choi, Acta Mater. **61**, 6132 (2013)
13. D. Raabe, M. Herbig, S. Sandlöbes, Y. Li, D. Tytko, M. Kuzmina, D. Ponge, P.-P. Choi, Curr Opin Solid State Mater Sc **18**, 253 (2014)
14. M. Herbig, D. Raabe, Y. J. Li, P. Choi, S. Zaefferer, S. Goto, Phys. Rev. Lett. **112**, 126103 (2014)
15. M.-M. Wang, C.C. Tasan, D. Ponge, A.-Ch. Dippel, D. Raabe, Acta Mater **85**, 216 (2015)
16. O. Dmitrieva, D. Ponge, G. Inden, J. Millán, J., P. Choi, J. Sietsma, D. Raabe, Acta Mater **59**, 364 (2011)
17. M. Belde, H. Springer, G. Inden, D. Raabe, D., Acta Mater **86**, 1 (2015)
18. M. Kuzmina, D. Ponge, D. Raabe, Acta Mater. **86**, 182 (2015).
19. M. Kuzmina, M. Herbig, D. Ponge, S. Sandlöbes, D. Raabe, submitted.
20. Z. Tarzimoghadam, S. Sandlöbes, K. G. Pradeep, D. Raabe, Acta Mater. in press (2015)